Constraint-Based Analysis of Parallel Kinematic Articulated Wrist Mechanisms

Revanth Damerla[1]
Precision Systems Design Laboratory,
Mechanical Engineering,
University of Michigan,
Ann Arbor, MI 48109
e-mail: damerla@umich.edu

Shorya Awtar
Precision Systems Design Laboratory,
Mechanical Engineering,
University of Michigan,
Ann Arbor, MI 48109
e-mail: awtar@umich.edu

This paper presents a systematic constraint-based analysis of the performance attributes of eight parallel kinematic articulated wrist mechanisms from the existing literature. These performance attributes include the number, nature (i.e., pure rotation, or translation, or a combination), and location of a mechanism's Degrees of Freedom (DoFs) in the nominal and displaced configurations, load transmission capability along these DoFs, and load-bearing capability along the constraint directions. This systematic analysis reveals performance tradeoffs between these performance attributes for a given mechanism as well as design tradeoffs across these mechanisms. This analysis also helps inform the suitability of a given mechanism for specific applications.
[DOI: 10.1115/1.4049947]

Keywords: mechanism design, mechanism synthesis, parallel platforms, compliant mechanisms

1 Introduction and Background

Articulated wrist mechanisms offer at least two rotations (commonly designated as pitch and yaw) and are used in an array of applications that require dexterous manipulation, remote access, or orientation adjustment. These applications include minimally invasive surgery [1–5], measuring displacements of a human interface for control [5–7], industrial operations such as robotic welding and spay-painting [8,9], handling of hazardous material [8,9], varying the orientation of a camera or other sensors in commercial [10,11] or aerospace [12,13] applications, varying the pointing angle of a fire extinguisher [14], and various robotic operations [15–19], to name a few. This wide range of applications has led to many unique articulated wrist mechanisms with various performance attributes, which determine the suitability of a mechanism for a given application.

These performance attributes include the Degrees of Freedom (DoFs) and Degrees of Constraint (DoCs) of an End Effector (EE) of a mechanism with respect to its Base (Fig. 1). DoFs are the independent directions of motion that the End Effector can undergo while DoCs are the independent directions that the End Effector is constrained to not move along. DoFs are geometrically represented by *freedom lines* that capture pure rotation, pure translation, or a combination (i.e., screw). Similarly, DoCs are represented by *constraint lines* that capture translational constraint, rotational constraint, or a combination (i.e., wrench). The freedom lines of a mechanism together form its freedom space, and similarly, all the constraint lines of a mechanism form its constraint space. The freedom and constraint spaces of a mechanism define how it moves and transmits loads.

Freedom lines and constraint lines follow certain basic rules of geometry: DoFs add in series, DoCs add in parallel, and they are complementary to each other. The latter, known as the Rule of Complementary Patterns [20], states that if there are n independent constraint lines, then there will be $6–n$ independent freedom lines, each of which will intersect every constraint line. Thus, the freedom and constraint spaces are complementary. This rule can be used to identify freedom spaces from constraint spaces and vice versa. Screw theory provides a mathematical representation of the same concepts, which is beneficial when the constraint and freedom spaces are challenging to visualize and analyze using straightforward geometric arguments [21–25]. The Freedom and Constraint Topology (FACT) framework builds upon these geometric and mathematical principles to provide a comprehensive catalog of all possible constraint and freedom spaces [26]. In this paper, we will make use of these tools to analyze freedom and constraint spaces.

An articulated wrist mechanism offers at least two rotational DoFs (pitch and yaw) between an End Effector and Base. Ideally, in the nominal or undisplaced configuration, the pitch and yaw axes are orthogonal (Fig. 1(*a*)). In this nominal configuration, it is helpful to construct a central axis that is orthogonal to both the pitch and yaw axes, passes through the point of intersection of these two axes, and is affixed to the End Effector. In a displaced configuration (Fig. 1(*b*)), the central axis retains its location with respect to the End Effector. Several performance attributes that impact the performance and suitability of an articulated wrist mechanism for a given application are compiled below and capture the scope of investigation in this paper.

(1) *Number of DoFs of the End Effector with respect to the Base in the nominal and displaced configurations.* The mechanism may exhibit redundant constraint lines in the nominal configuration that become non-redundant in a displaced configuration, or vice versa, resulting in a change in the number of DoFs.
(2) *Location of the DoFs in the nominal and displaced configurations.* Change in location can mean that, upon displacement of the mechanism from its nominal configuration, the pitch and yaw rotational DoFs no longer remain in the same plane, or remain orthogonal, or intersect at the same point, or intersect at all, or a combination of these. Drifting of these pitch and yaw freedom lines with increasing displacement implies that the End Effector will not trace a perfect hemisphere.
(3) *Nature of the DoFs in the nominal and displaced configurations.* Change in nature can mean that the two DoFs (pitch and yaw) no longer remain purely rotational and instead have a coupled translational component (i.e., screw

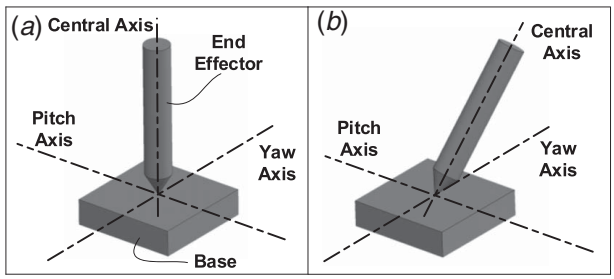

Fig. 1 Generic Articulated Wrist Mechanism: (*a*) nominal configuration and (*b*) displaced configuration

[1]Corresponding author.
Contributed by the Mechanisms and Robotics Committee of ASME for publication in the Journal of Mechanisms and Robotics. Manuscript received September 8, 2020; final manuscript received January 20, 2021; published online March 12, 2021. Assoc. Editor: Leila Notash.

motion). This also implies that the End Effector will not trace a perfect hemisphere.

(4) The articulated wrist mechanism is intended to bear loads along DoC directions, and therefore, *load-bearing capability (or equivalently stiffness)* in these directions is critical. This is impacted by the mechanism's kinematics (e.g., transmission angles) and construction (e.g., joint or link stiffness), both of which can vary from nominal to displaced configurations.

(5) If the articulated wrist mechanism is used in an active application where loads are transmitted from actuated inputs at the Base (e.g., pitch and yaw input) to the End Effector output, then *load transmission capability (or equivalently transmission stiffness)* becomes critical. This is also impacted by the kinematics and construction of the mechanism and can vary from nominal to displaced configurations.

As noted above, these performance attributes typically deviate from nominal behavior with increasing displacement of the mechanism, thereby potentially creating performance tradeoffs between these attributes and the range of motion. Range of motion is also impacted by practical considerations such as the sizes of links and joints and collisions between them.

An articulated wrist mechanism can be either serial or parallel kinematic in its architecture. Parallel kinematic mechanisms allow for ground-mounted actuators, making them preferable in active applications. They can also be more compact and lightweight, resulting in faster speeds. However, their design and evaluation (qualitative as well as quantitative) is more complex [10,20–28]. Because of these reasons along with their wide applicability, we focus on parallel kinematic articulated wrist mechanisms in this paper. We identify eight mechanisms from the literature (see Fig. 2) and present a systematic and comprehensive constraint-based analysis that identifies the number, location, and nature of the DoFs of each mechanism in the nominal and displaced configurations. We also present a qualitative analysis that leverages the results of the constraint-based analysis to identify tradeoffs between certain features of the mechanisms and load-bearing and transmission capabilities, range of motion, or a combination. These combined analyses generate insights into performance tradeoffs (within a given mechanism) and design tradeoffs (between the various mechanisms).

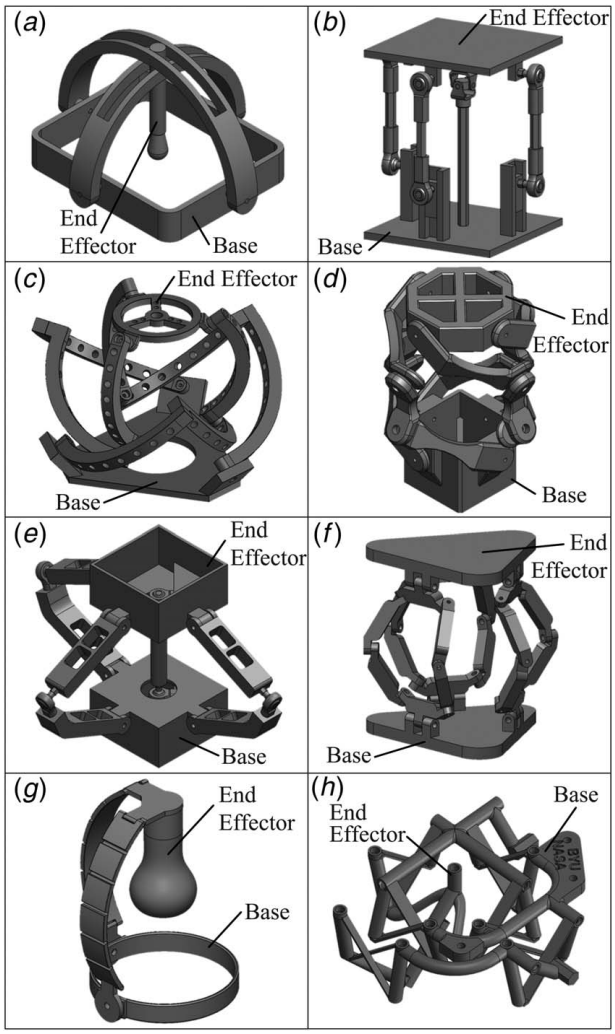

Fig. 2 Parallel kinematic articulated wrist mechanisms: (*a*) Dual Arch, (*b*) Tip-Tilt Plate, (c) Agile Eye, (*d*) OmniWrist III, (e) OmniWrist V, (*f*) Three-Spherical Kinematic Chain Parallel Mechanism, (*g*) FlexDex, and (*h*) BYU Space Pointing Mechanism

These mechanisms were chosen primarily for their diversity in architecture, performance, and applications. As a result, they provide a representative set of the design tradeoffs that can be expected within parallel kinematic articulated wrist mechanisms. The Dual Arch [3,5–7] (Fig. 2(*a*)), Tip-Tilt Plate [18] (Fig. 2(*b*)), and Agile Eye [10] (Fig. 2(*c*)) mechanisms are composed entirely of rigid joints and links. These mechanisms offer ideal pitch and yaw DoFs, meaning they remain pure rotations and retain their intersection point even after displacement. The next three mechanisms are the OmniWrist III [14,29] (Fig. 2(*d*)), OmniWrist V [30] (Fig. 2(*e*)), and Three-Spherical Kinematic Chain Parallel Mechanism [1,28] (Fig. 2(*f*)), which are also entirely composed of rigid links and joints. However, their pitch and yaw DoFs do not remain purely rotational upon displacement. Next, the FlexDex® mechanism [4,5] (Fig. 2(*g*)) is shown to offer pitch and yaw DoFs under the assumption of compliance in certain links and joints. Finally, the BYU Space Pointing mechanism [12] (Fig. 2(*h*)) is a monolithic mechanism composed of rigid links and compliant joints. The compliance enables pitch and yaw DoFs, which may not retain their nominal behavior.

2 Constraint-Based Analysis of Articulated Wrist Mechanisms

The convention of illustrating constraint and freedom lines used throughout this paper is as follows. Red dashed straight lines are used to indicate rotational DoFs while translational DoFs are shown as red dashed circles that are understood to be of infinite radius. The direction of translation is along the line normal to the plane of this circle. Screw DoFs are shown as solid green lines. Pure translational constraint lines are shown as solid blue lines. Black lines are used occasionally to denote axes of interest and are not meant to indicate any DoFs or DoCs. Letters F and C denote freedom and constraint lines, respectively, and numbers provide further specification. For example, $F1_2$ represents the second freedom offered by the first chain in the mechanism. Additional nomenclature includes Base (B), End Effector (EE), revolute joint (R), prismatic joint (P), spherical joint (S), and sliding joint (J). Unless otherwise specified, all links and joint are assumed to be ideal—the links are infinitely stiff in all directions, the joints are infinitely stiff in DoC directions, and the joints have zero stiffness in their DoF directions. Further explanation of the freedom and constraint analyses for each of the following mechanisms can be found in related publications [31,32].

2.1 Dual Arch Mechanism. The Dual Arch mechanism consists of two identical serial chains: B-R1-L1-J1-EE and B-R2-L2-J2-EE (Fig. 3(*a*)). The freedom and constraint spaces associated with the first chain are shown in Fig. 3(*b*). It can be shown that the first chain contributes $C1_1$ to the overall mechanism. This constraint line is parallel to the freedom lines $F1_2$, $F1_3$, and $F1_4$ and passes through the intersection of $F1_1$ and $F1_5$.

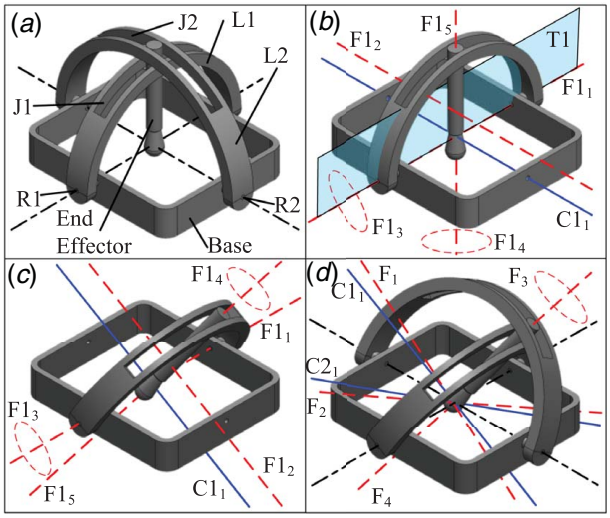

Fig. 3 Dual Arch: (*a*) full mechanism nominal configuration, (*b*) first chain nominal configuration, (c) first chain displaced configuration, and (*d*) full mechanism displaced configuration

Figure 3(*c*) illustrates the freedom and constraint spaces of the first chain when the arch has been rotated about the revolute joint R1. The constraint line $C1_1$ in this displaced configuration remains parallel to the displaced $F1_2$, $F1_3$, and $F1_4$ and passes through the intersection of $F1_1$ and $F1_5$.

The second chain is orthogonal to the first chain in placement but identical in structure. Constraint $C2_1$ contributed by the second chain intersects $C1_1$ at the same point as the intersection point of the R1 and R2 revolute joint axes (black centerlines). When the End Effector has been rotated in both pitch and yaw, the two constraint lines $C1_1$ and $C2_1$ for the overall mechanism continue to intersect at the intersection point of the R1 and R2 joint axes. As a result, three independent DoFs F_1, F_2, and F_4 for the overall mechanism also pass through this intersection point, in any displaced configuration, and form a freedom space that is similar to an ideal spherical joint. Another freedom line F_3, located at infinity, represents the translation of the End Effector along the central axis.

Thus, this mechanism can be used as a four DoFs mechanism or it can be reduced to an articulated wrist mechanism with only pitch and yaw DoFs F_1 and F_2. F_3 can be removed by constraining the End Effector with respect to either or both Arch Links in translation along the central axis, while F_4 can be removed by introducing a rotational constraint between the End Effector and any one (but not both) of the sliding joints. With these additional constraints in place, the two remaining DoFs, F_1 and F_2, lie in the plane normal to the central axis in any displaced configuration. The intersection point of these two freedom lines also does not drift from the intersection point of R1 and R2 joint axes.

This mechanism has a relatively compact and simple structure, but its range of motion is limited by singular configurations when the End Effector reaches 90 deg in any direction. When the mechanism is increasingly articulated in pitch or yaw, the approaching singularity causes a loss in transmission ratio in the other rotational DoF. This means that the End Effector can no longer be actuated along the second DoF. As the transmission ratio drops, the mechanical advantage goes up, which can be beneficial for load transmission. Load-bearing capabilities along the DoCs are similarly affected as the mechanism moves from its nominal to a displaced configuration. When the mechanism is articulated in one DoF (e.g., corresponding to R1 joint), the translational DoC along the R1 axis becomes stronger because the End Effector moves closer to the Base and therefore the R2 joint, which supports this DoC. Physical limitations like collisions and singularities prevent it from tracing out an entire hemisphere, but it can trace a section of a perfect hemisphere. Within this continuous but finite range of motion, the load transmission and bearing capabilities are dictated more by the geometry and construction of the various rigid links and joints. Furthermore, this mechanism offers a large open space around the intersection of the pitch and yaw axes, making this mechanism suitable not only for pointing and tracking applications, but also applications that require a remote center of rotation located in an open space [3,5–7,15].

2.2 Tip-Tilt Plate Mechanism. The Tip-Tilt Plate mechanism is part of a group of mechanisms similar to the Stewart platform but with fewer DoFs. The particular version shown in Fig. 4(*a*), which is 3PSS + U [18], comprises three outer chains, the first with structure B-$P1_1$-$L1_1$-$S1_1$-$L1_2$-$S1_2$-EE, and one central chain with structure B-$R4_1$-$L4_1$-$R4_2$-EE.

The freedom space of the first outer serial chain in the nominal configuration is shown in Fig. 4(*b*). $P1_1$ provides the DoF $F1_1$, while $S1_1$ provides $F1_2$, $F1_3$, and $F1_4$. $S1_2$ also provides $F1_4$ as well as $F1_5$ and $F1_6$. The freedom space of this serial chain, therefore, provides six independent DoFs and has no DoCs.

The freedom and constraint spaces of the central chain are shown in Fig. 4(*c*). $R4_1$ and $R4_2$ provide the DoFs $F4_1$ and $F4_2$, respectively. Since these two revolute joints form a universal joint, the freedom lines intersect at a point along the central axis. The corresponding constraint space is composed of four constraint lines. $C4_1$, $C4_2$, and $C4_3$ intersect the same point as the two freedom lines and are not coplanar. $C4_4$ lies in the same plane as $F4_1$ and $F4_2$ but does not pass through their intersection.

Since the central chain is the only chain with any DoCs, the constraint space of the mechanism is identical to the central chain's in both the nominal and displaced configurations as shown in Fig. 4(*d*). The mechanism, therefore, has two DoFs F_1 and F_2 that are coplanar to $F4_1$ and $F4_2$ and share the same intersection point. While the two freedom lines do not remain in the same plane as the End Effector, their intersection does not drift, and their nature does not change in any displaced configuration. This mechanism can therefore trace out a portion of a hemisphere but is typically limited in range of motion by the joints it is composed of. In cases where joint capabilities do not limit performance, physical limitations such as link thickness prevent this mechanism from tracing an entire hemisphere.

Load transmission and load-bearing capabilities are similarly limited by the capabilities of the joints but can be made very large by increasing their size along with the links. The central

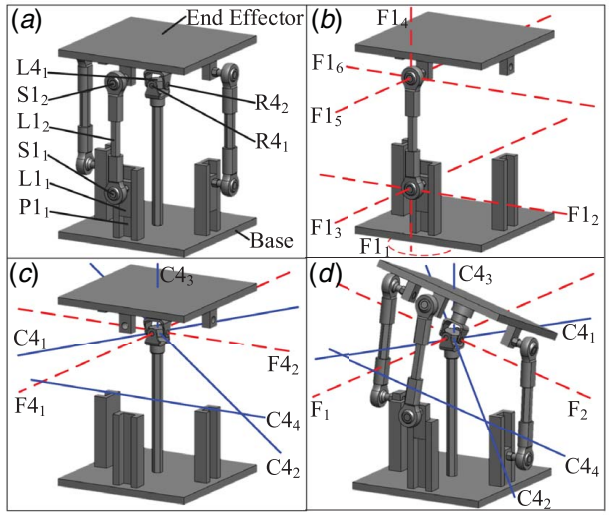

Fig. 4 Tip-Tilt Plate: (*a*) full mechanism nominal configuration, (*b*) first outer chain nominal configuration, (c) central chain nominal configuration, and (*d*) full mechanism displaced configuration

chain is especially important to these capabilities since it provides the four DoCs of the mechanism. Although the outer chains do not provide any DoCs, they are important because they provide the opportunity to have independent ground-mounted actuation for each DoF. In this mechanism, this can be done by interfacing the prismatic joints in two orthogonal outer chains with linear actuators. The third outer chain as well as any additional outer chains are redundant but would provide the ability to use multiple actuators for a single EE DoF.

There are several other variations of this mechanism, which can have different outer chains (e.g., SPS [18], UPS [2,19], and RSS [16,17]) and/or different central chains (e.g., S [2,17,33] and PS [18]). These variations will preserve the mechanism's pitch and yaw (i.e., tip and tilt) capabilities but may offer additional DoFs. Depending on the variation, rotary actuators may be used (e.g., at the revolute joint of RSS chains). The performance attributes of the 3PSS + U mechanism are attractive for a wide range of applications, including in pointing and tracking applications, rehabilitative robotics, minimally invasive surgery, and additional applications that require large loads. However, the arrangement of its central chain means there is no virtual center; it therefore is not suitable for applications requiring one.

2.3 Agile Eye Mechanism. The Agile Eye mechanism is representative of a class of 3RRR spherical parallel kinematic manipulators capable of pitch, yaw, and roll rotations. Numerous other examples of mechanisms with the same kinematic architecture exist within the literature [10,27,34]. However, the Agile Eye stands apart because its geometry enables a relatively large workspace that can be arranged to avoid singularities [10,34].

This mechanism is composed of three identical serial chains. The structure of the first serial chain, highlighted in pink in Fig. 5(*a*), is B-$R1_1$-$L1_1$-$R1_2$-$L1_2$-$R1_3$-EE. The most important physical detail of this mechanism is that the axes of rotation of all nine revolute joints always intersect the same point in space regardless of displacement. The constraint and freedom spaces of the first chain in the nominal and displaced configuration are shown in Figs. 5(*b*) and 5(*c*), respectively. These illustrate the second important physical detail of the Agile Eye: the links are arranged such that $F1_1$ and $F1_2$ are orthogonal and $F1_2$ and $F1_3$ are also orthogonal. In most nominal and displaced configurations, $F1_1$, $F1_2$, and $F1_3$ intersect the same point but are not coplanar; however, the mechanism becomes singular when $F1_1$ and $F1_3$ are collinear and the three freedom lines are coplanar. In nonsingular configurations, the serial chain has three constraint lines $C1_1$, $C1_2$, and $C1_3$ that also intersect the same point and are not coplanar. Since the freedom lines of all three chains share the same intersection point, there are six redundant DoCs. The overall mechanism's constraint and freedom spaces in the displaced configuration are shown in Fig. 5(*d*). The mechanism's freedom space is like an ideal spherical joint. If the mechanism is designed carefully, the freedom space remains unchanged throughout the mechanism's workspace [10]. However, some versions of this mechanism can contain singular configurations, leading to either uncontrolled DoFs or a loss of ability to actuate the End Effector in certain directions [34].

The strict geometric requirements of joint DoFs and complex intertwined architecture that are required place unique practical limitations on this mechanism's performance. Apart from any singularities that can typically be avoided, the reachable workspace in all three DOFs is dictated by collisions between the links and is therefore inversely related to their size (e.g., thickness). Similarly, load transmission and load-bearing capabilities are directly related to the size and stiffness of the links. One instance of this mechanism has been shown to achieve a workspace of a 140 deg cone of constant radius with ±30 deg in roll [10]. This mechanism does not offer a large open space around the virtual center over its entire range of motion. This makes it more suitable for fast pointing and tracking applications than for human interface applications.

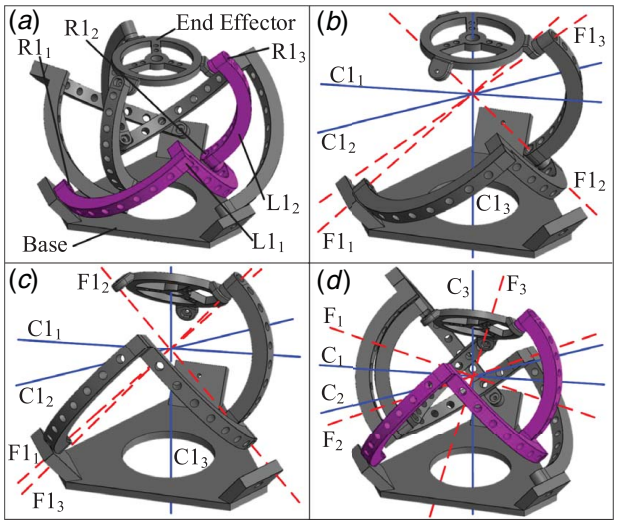

Fig. 5 Agile Eye: (*a*) full mechanism nominal configuration, (*b*) first chain nominal configuration, (*c*) first chain displaced configuration, and (*d*) full mechanism displaced configuration (Color version online.)

2.4 OmniWrist III Mechanism. OmniWrist mechanisms offer large ranges of singularity-free motion [8,11,30]. The OmniWrist III is one such example that in its most basic form, consists of three identical chains that are wrapped around the End Effector. However, additional chains can be added while preserving the freedom space. Accordingly, we present a four-chain version of the OmniWrist III in Fig. 6. The structure of the first chain, highlighted in pink in Fig. 6(*a*), is B-$R1_1$-$L1_1$-$R1_2$-$L1_2$-$R1_3$-$L1_3$-$R1_4$-EE.

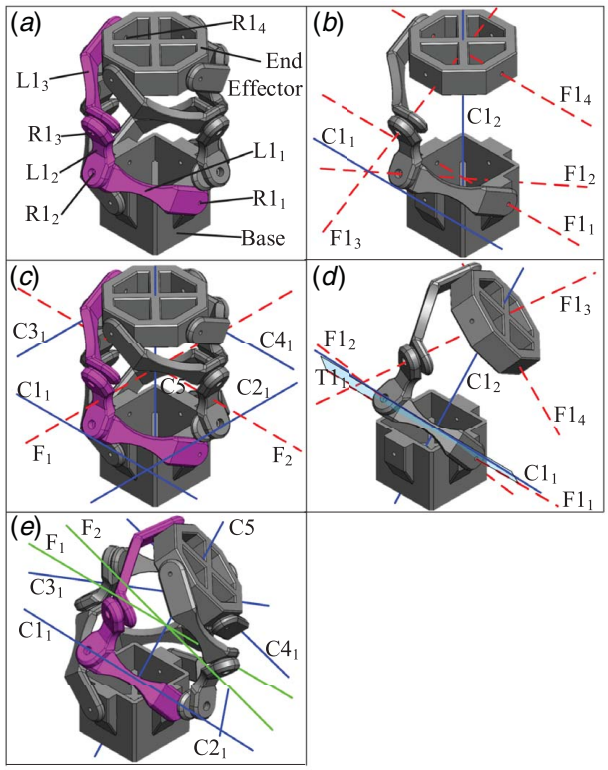

Fig. 6 OmniWrist III: (*a*) full mechanism nominal configuration, (*b*) first chain nominal configuration, (*c*) full mechanism nominal configuration, (*d*) first chain displaced configuration, and (*e*) full mechanism displaced configuration (Color version online.)

The freedom and constraint spaces of the first chain in the nominal configuration are shown in Fig. 6(*b*). The most important feature of this mechanism is that $F1_1$ and $F1_2$ intersect at a point at the center of the Base and $F1_3$ and $F1_4$ intersect at the center of the End Effector. This is possible because of the special construction of links $L1_1$ and $L1_3$, which are identical; the two intersection points remain in the same location with respect to the Base and End Effector regardless of mechanism orientation. $C1_2$ is the line that connects these two points. $F1_2$ and $F1_3$ also intersect at a point outside of the mechanism because of the special construction of $L1_2$. $C1_1$ is the line that passes through this latter intersection point and is also parallel to $F1_1$ and $F1_4$.

The constraint and freedom spaces of the overall mechanism in the nominal configuration are shown in Fig. 6(*c*). C_5 is collectively composed of the $C1_2$, $C2_2$, $C3_2$, and $C4_2$, which are redundant. Since $C1_1$, $C2_1$, $C3_1$, and $C4_1$ are coplanar, one of the constraints is redundant. The mechanism, therefore, has four independent constraints and produces the freedom space of F_1 and F_2 that are coplanar to $C1_1$, $C2_1$, $C3_1$, and $C4_1$ and intersect C_5. This freedom space represents the pitch and yaw rotations of an articulated wrist mechanism. However, it does not maintain this freedom space in displaced configurations.

Figure 6(*d*) shows the freedom and constraint spaces of the first chain in a displaced configuration. $F1_1$, $F1_2$, and $F1_3$ maintain similar relationships to each other, while $F1_4$ rotates along with the End Effector. As a result, $F1_4$ is no longer parallel to $F1_1$ and a more complex process to identify and locate $C1_1$ in displaced configurations is needed [31]. While the orientation of $F1_4$ changes relative to $F1_1$, the important freedom line intersection points are preserved as expected. Thus, $C1_2$ still passes through the same points on the Base and End Effector.

Since $C1_1$, $C2_1$, $C3_1$, and $C4_1$ are no longer coplanar and have more complicated relationships, it is difficult to draw the corresponding freedom space. It is, therefore, simpler to use screw theory directly to conduct the constraint analysis. This was accomplished by following the methods described in [23–25] but with joint locations determined numerically using a CAD model of the mechanism. The constraint and freedom spaces in the displaced configuration are shown in Fig. 6(*e*). C_5 still collectively represents the redundant constraint lines $C1_2$, $C2_2$, $C3_2$, and $C4_2$. The mechanism's freedom space is composed of two screws that appear to intersect each other and remain perpendicular to C_5. The intersection point also remains a constant distance from the End Effector, meaning that while the nature of the DoFs changes, their location does not drift. However, given the numerical approach used to determine the freedom space, these attributes could not be confirmed geometrically. The FACT catalog helps to identify the constraint space as nested circular hyperboloids [26]. This reveals that any number of serial chains can be used as long as the symmetries needed to produce this freedom space are maintained.

Because its freedom space comprises two intersecting screws in displaced configurations, the OmniWrist III is unable to trace out a perfect hemisphere. However, it can trace out an oblong hemisphere (full 180 deg) while remaining free of singularity. The mechanism's range of motion is determined by collisions between links from different chains. This results in a tradeoff between link dimensions (e.g., thickness) and range of motion. To maximize range of motion, the links must be compact. This can result in finite stiffness of the supposedly rigid links, which adversely impacts load-bearing and transmission capabilities. In particular, the load-bearing capability along C_5 is sensitive since it depends on the bending stiffness of the links. These features and tradeoffs make this mechanism a promising candidate in applications including pointing, tracking, and manufacturing. In the latter application, a robotic arm supporting the mechanism can make up for the small translations caused by the screw DoFs. It is also possible to arrange the serial chains to create an open space around the virtual center, potentially at the cost of load-bearing capability. This mechanism can therefore also be used in applications that require a human interface.

2.5 OmniWrist V Mechanism. While the OmniWrist V may appear architecturally different from the OmniWrist III, a constraint-based analysis reveals the similarities between these two mechanisms. An example is shown in Fig. 7(*a*) and consists of two different types of chains. The first chain is an example of the outer chain, with structure B-$R1_1$-$L1_1$-$S1_1$-$L1_2$-$R1_2$-EE. The fourth chain is the central chain, with structure B-$S4_1$-$L4_1$-$S4_2$-EE.

The freedom and constraint spaces of the first outer chain in the nominal configuration are shown in Fig. 7(*b*). $R1_1$ provides the freedom line $F1_1$, spherical joint $S1_1$ provides $F1_2$, $F1_3$, and $F1_4$, and $R1_2$ provides $F1_5$; this adds to a total of five DoFs. The corresponding constraint line $C1_1$ must pass through the center of $S1_1$ to intersect $F1_2$, $F1_3$, and $F1_4$; it also must run parallel to $F1_1$ and $F1_5$.

The freedom and constraint spaces of the central chain in the nominal configuration are shown in Fig. 7(*c*). Both $S4_1$ and $S4_2$ provide three DoFs. However, one of the DoFs is redundant and is represented by the shared freedom line $F4_3$. $C4_1$ is the line drawn between the centers of the two joints. This relation holds throughout the mechanism's workspace.

The mechanism constraint and freedom spaces in the nominal configuration are shown in Fig. 7(*d*). This reveals that the constraint lines formerly provided by a single serial chain in the OmniWrist III are decoupled into two separate chains in this mechanism. The outer serial chains provide constraint lines similar to $C1_1$ in the OmniWrist III, while C_5 is now provided by a single central chain. $C1_1$, $C2_1$, and $C3_1$ are coplanar in the nominal configuration, and therefore, any two freedom lines lying within the same plane and also intersecting $C4_1$ can be chosen. Thus, this mechanism also provides pure pitch and yaw rotational DoFs in the nominal configuration but does not maintain this freedom space in displaced configurations.

The freedom and constraint spaces for the first outer chain in a displaced configuration are shown in Fig. 7(*e*). While links $L1_1$

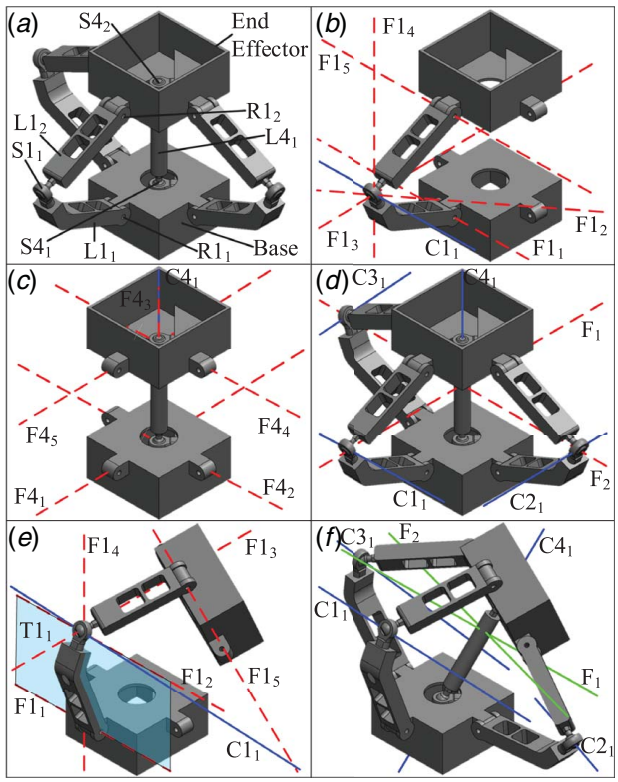

Fig. 7 OmniWrist V: (*a*) full mechanism nominal configuration, (*b*) first outer chain nominal configuration, (c) central chain nominal configuration, (*d*) full mechanism nominal configuration, (e) first chain displaced configuration, and (*f*) full mechanism displaced configuration

and $L1_2$ become displaced, the relative orientations of $F1_1$, $F1_2$, $F1_3$, and $F1_4$ all maintain similar relationships to each other. However, the orientation of $F1_5$ rotates to maintain its relation to the displaced End Effector. As a result, a similar approach to what was needed for the OmniWrist III should be used [31].

As with the OmniWrist III, the changes to the orientations of $C1_1$, $C2_1$, and $C3_1$ mean they are no longer coplanar. A numerical analysis analogous to that used for the OmniWrist III reveals that the corresponding freedom space now consists of two screw lines that appear to intersect each other and $C4_1$ as shown in Fig. 7(*f*). In addition, the plane comprising these two screw lines appears normal to $C4_1$ and does not drift in any displaced configurations. These attributes of the freedom space were again observed via a numerical analysis and were not confirmed geometrically. The FACT catalog helps identify the constraint space as nested circular hyperboloids, as with the OmniWrist III [26].

The appearance of screw lines means that this mechanism is also unable to trace out a perfect hemisphere. The central chain plays a critical role in the range of motion of this mechanism, which can be dictated by the spherical joints $S4_1$ and $S4_2$. For the End Effector to span its full hemispherical range, these spherical joints must together provide 90 deg of rotation from their nominal configuration. Unlike with the OmniWrist III, in general, high load bearing along DoCs can be achieved via adequately stiff links and joints in the mechanism because of few geometric limitations; links can be made thicker for little cost beyond additional mass. In addition, the decoupling of DoCs into two different types of chains means that the central chain can provide significant load bearing capability along constraint line $C4_1$ because $L4_1$ is either in tension or compression instead of in bending. This mechanism is therefore better suited for applications requiring high load-bearing and transmission stiffness than the OmniWrist III. This makes the mechanism a great candidate for pointing or tracking applications as well as for manufacturing applications such as welding and spray painting. However, the central chain envelops the intersection of the freedom lines and it therefore cannot be used for applications requiring a remote center of rotation located in an open space.

The outer chains in this mechanism can also be spaced 120 deg apart instead of 90 deg. Furthermore, as with the OmniWrist III, this architecture allows for the inclusion of additional outer chains, which would be redundant and would not alter the freedom space of the mechanism in any configuration. For example, the OmniWrist VI has a very similar structure compared with the OmniWrist V but includes four outer chains instead of three. Thus, the OmniWrist VI will have improved load-bearing capabilities due to the additional stiffness of a fourth chain.

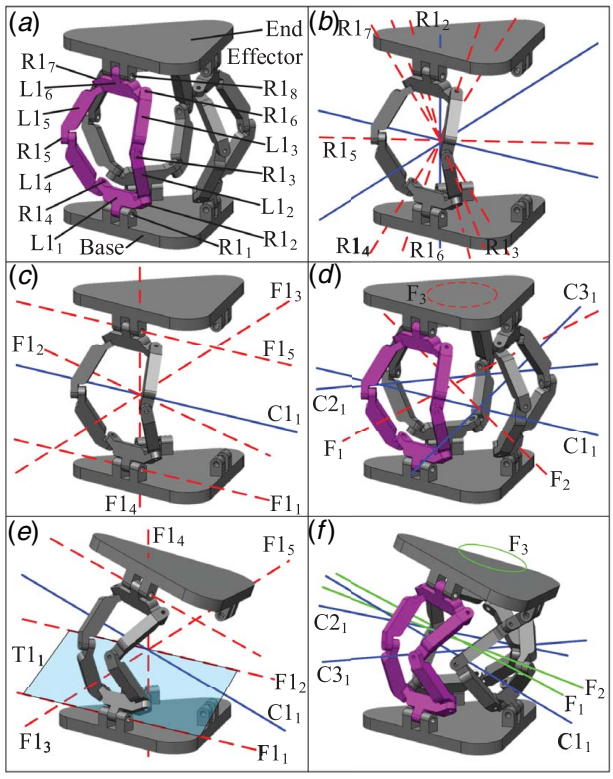

Fig. 8 Three-Spherical Kinematic Chain Parallel Mechanism: (*a*) full mechanism nominal configuration, (*b*) first chain's spherical parallel sub-chain nominal configuration, (c) first chain nominal configuration, (*d*) full mechanism nominal configuration, (e) first chain displaced configuration, and (*f*) full mechanism displaced configuration (Color version online.)

2.6 Three-Spherical Kinematic Chain Parallel Mechanism. This mechanism bears similarities to both OmniWrist mechanisms, especially the OmniWrist V because of a similar chain. It comprises at least three identical serial-parallel hybrid chains as shown in Fig. 8. The first chain, highlighted in pink (Fig. 8(*a*)), has the following structure:

$$B - R1_1 - L1_1{}^{-R1_2-L1_2-R1_3-L1_3-R1_6-}_{-R1_4-L1_4-R1_5-L1_5-R1_7-}L1_6 - R1_8 - EE$$

The freedom and constraint spaces of the first chain's spherical parallel sub-chain, composed of $R1_2$-$L1_2$-$R1_3$-$L1_3$-$R1_6$-$L1_6$ and $R1_4$-$L1_4$-$R1_5$-$L1_5$-$R1_7$-$L1_6$, are shown in Fig. 8(*b*). The geometry of the two serial chains makes the sub-chain kinematically equivalent to a spherical joint. This is true except when the DoFs of one of the serial chains are coplanar as this will lead to a loss a DoF. The constraint and freedom spaces of the first chain in the nominal configuration are shown in Fig. 8(*c*). These reveal that the chain is kinematically equivalent to the OmniWrist V's outer chain, with the spherical joint replaced by the spherical parallel sub-chain.

Figure 8(*d*) shows the constraint and freedom spaces of the overall mechanism. Each serial chain provides a single constraint line; the three constraint lines are coplanar but do not share a single intersection point. Therefore, none are redundant and the mechanism has three corresponding DoFs; a singularity occurs if this condition is not met. This is possible upon displacement if the spherical centers of the three sub-chains become coincident. When the mechanism is nonsingular, the three DoFs can represent pitch, yaw, and vertical translation.

As with the OmniWrist mechanisms, the freedom space of the mechanism changes significantly in displaced configurations. The freedom and constraint spaces of the first serial chain after it has displaced from the nominal configuration in pitch and yaw but not in translation are shown in Fig. 8(*e*). Assuming the spherical parallel sub-chain has not lost a DoF, the serial chain still provides five DoFs. A similar approach to the one used in the OmniWrist V is then used to construct $C1_1$.

The constraint lines of the three chains are no longer coplanar when the mechanism is displaced in pitch and yaw without translation. As with the OmniWrist mechanisms, it is convenient to use screw theory to numerically find the corresponding freedom space, shown in Fig. 8(*f*). This analysis shows that the freedom space is composed of three screw lines, of which two screw lines F_1 and F_2 appear to intersect. These screw lines are analogous to the pitch and yaw DoFs in the nominal configuration. The appearance of these screw lines in displaced configurations means that the mechanism is unable to trace a perfect hemisphere. The third screw line, F_3, is analogous to the translational DoF and has a very high pitch, unlike the other two screw DoFs. From this pure pitch and yaw displaced configuration, if the mechanism is now displaced in translation, the above described freedom and constraint spaces will no longer apply.

The FACT catalog reveals that this arrangement of three screw DoFs corresponds to a constraint space that takes the shape of a

single circular hyperboloid [26]. This only differs from the OmniWrist mechanisms because of the absence of an additional constraint line belonging to a nested circular hyperboloid. This was provided by the central chain in the OmniWrist V and its analogs in the OmniWrist III. However, F_3 could be removed with the addition of a chain like the OmniWrist V's central chain or by removing symmetry when a fourth chain is added. The catalog also reveals that an identical fourth chain arranged correctly would be redundant since the constraint line it provides would also be a part of the same circular hyperboloid.

Replacing the OmniWrist V outer chain's spherical joint with the spherical parallel sub-chain has several consequences that lead to clear differences between the two mechanisms. The sub-chains can have improved stiffness because of their revolute joints and parallel architecture. In addition, they do not change the overall kinematic behavior of the mechanism in most displaced configurations. However, the mechanism's range of motion is limited by several factors related to the sub-chain including locations leading to loss of DoFs or link collisions. There is therefore a tradeoff between range of motion and load-bearing and transmission capabilities as these depend on the stiffness and, therefore, size of the links and joints. Thus, its set of performance tradeoffs is more like that of the OmniWrist III than the OmniWrist V despite its kinematic structure.

This mechanism is well-suited for applications that require a virtual center located in an open space. It is also suitable for pointing and tracking applications; one instance of this mechanism demonstrated a range of motion of 15 deg–27 deg in pitch and yaw in similar applications [1].

2.7 FlexDex® Mechanism. The FlexDex mechanism offers constraint and freedom spaces similar to the Dual Arch mechanism but highlights many advantages of compliant elements. This mechanism comprises two identical chains. The structure of the first chain, shown in Fig. 9(*a*), is B-$R1_1$-$L1_1$-$R1_2$-$L1_2$-$R1_3$-EE. $L1_2$ is a compliant strip composed of alternating "rigid" sections and "compliant" hinges. These compliant hinges are initially modeled as ideal revolute joints ($H1_1$, $H1_2$, and so on). While an ideal revolute joint has zero motion and infinite stiffness along its DoCs, in practice, a compliant hinge will have finite compliance along its DoF and finite stiffness and parasitic error motion along its DoCs. Similarly, the rigid sections are modeled initially as being ideal (i.e., infinitely stiff) but can have finite stiffness in practice.

The freedom and constraint spaces of the first chain in the nominal configuration are shown in Fig. 9(*b*). Each revolute joint and compliant hinge provides a single DoF as expected. An important feature of the complaint strip $L1_2$ is that the nominal axis of rotation of each compliant hinge is parallel to those of $R1_2$ and $R1_3$. The compliant hinges therefore provide DoFs that are parallel to $F1_2$ and $F1_4$. However, only a maximum of three of these parallel freedom lines are independent (when the strip is curved, as shown, and not flat) and the redundant DoFs provided by the compliant hinges can be ignored. The geometry of the FlexDex mechanism (i.e., the length and orientation of the two compliant strips) ensures that these strips are always curved. Thus, the first chain provides freedoms $F1_1$, $F1_2$, $F1_3$, and $F1_4$ and the corresponding constraint space comprises two lines $C1_1$ and $C1_2$ that are parallel to $F1_2$, $F1_3$, and $F1_4$ and intersect $F1_1$ (Fig. 9(*b*)). This freedom space is similar to the Dual Arch mechanism, except for the absence of the fifth DoF $F1_5$.

Analogous freedom and constraint spaces can be created for the second chain as well. The resulting constraint and freedom spaces of the overall mechanism in the nominal configuration are shown in Fig. 9(*c*). Since the four constraint lines are coplanar, only three of them are independent. This produces the corresponding freedom space with F_1, F_2, and F_3 that lie in the same plane and do not share the same intersection point. These can be arranged such that F_1 and F_2 correspond to pitch and yaw motions and F_3 corresponds to translation along the central axis. This is the expected

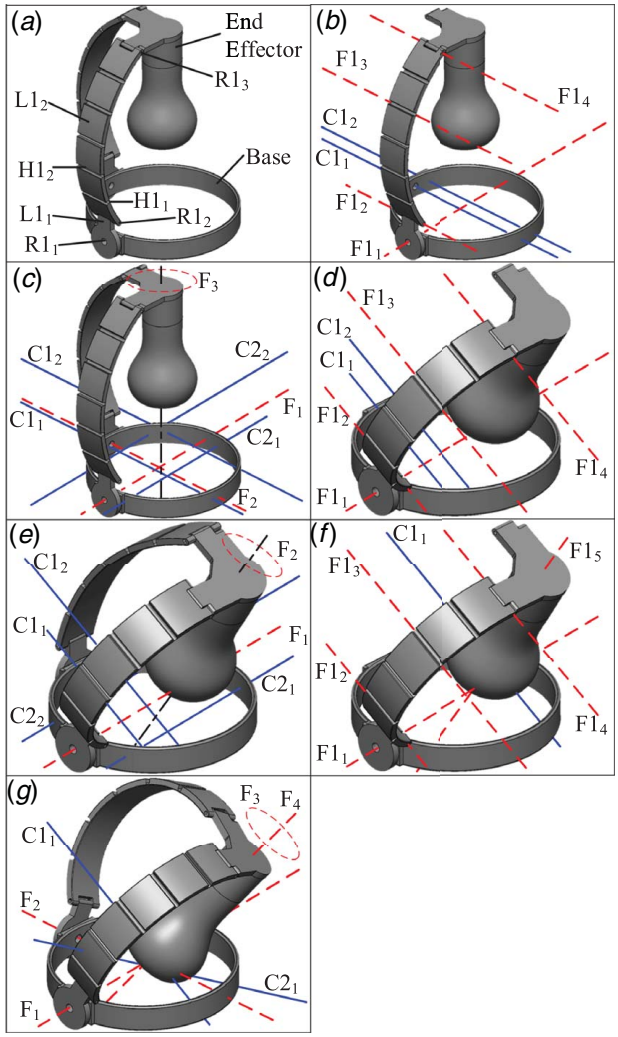

Fig. 9 FlexDex mechanism: (*a*) full mechanism nominal configuration, (*b*) first chain nominal configuration, (c) full mechanism nominal configuration, (*d*) first chain after single rotation, (e) full mechanism after single rotation, (*f*) modified freedom space for first chain after single rotation, and (*g*) full mechanism after both rotations

freedom space of an articulated wrist mechanism with an additional translational DoF.

The freedom and constraint spaces of the first chain after the chain has rotated about the $R1_1$ joint are shown in Fig. 9(*d*). While $F1_1$ remains in place, freedom lines $F1_2$, $F1_3$, and $F1_4$ rotate along with the rotation of the $R1_1$ revolute joint. $C1_1$ and $C1_2$ still intersect $F1_1$ but also rotate in order to remain parallel to $F1_2$, $F1_3$, and $F1_4$. The constraint and freedom spaces of the overall mechanism after the first chain has rotated about $F1_1$ are shown in Fig. 9(*e*). The mechanism constraint space now contains four constraint lines that do not lie in a single plane and are therefore no longer redundant. As a result, the mechanism's freedom space devolves into a two DoFs space where the freedom lines are parallel to $C2_1$ and $C2_2$ and intersect both $C1_1$ and $C1_2$. These two freedom lines can be arranged so that F_1 corresponds to continued rotation about the same axis (i.e., $F1_1$) and F_2 corresponds to translation along the central axis. The loss of DoF is critical in this case because the mechanism is no longer an articulated wrist mechanism. However, this analysis is based on an ideal constraint assumption for the compliant hinges and revolute joints, and ideal rigid sections and links.

In practice, the compliant strips are not ideal and compliance is advantageously employed to introduce intentional deviation from

ideal behavior. In particular, their "rigid" sections and compliant hinges have small but finite compliance in torsion, which plays an important role in providing the desired articulation functionality, as demonstrated in practical use [4,5].

With this knowledge and some modified assumptions, we can analyze the freedom and constraint spaces again. Most importantly, even though torsion is not truly a DoF for the compliant strip, we introduce the freedom line $F1_5$ to recognize the small but finite compliance in this direction. It is logical to place this additional freedom line collinear to the central axis because of the symmetry of the mechanism, although it can be located elsewhere depending on the geometric details of the compliant strip. With this assumption, the resulting freedom and constraint spaces of the first chain after it has rotated about the freedom $F1_1$ are shown in Fig. 9(*f*). This freedom space is identical to the freedom space of the first chain in the Dual Arch in a displaced configuration. The addition of $F1_5$ removes one of the two constraint lines present in Fig. 9(*d*). $C1_1$ must now pass through the intersection of $F1_1$ and $F1_5$.

Making a similar nonideal assumption for the second compliant strip, the constraint and freedom spaces of the overall mechanism after both chains have rotated about $F1_1$ and $F2_1$, respectively, are shown in Fig. 9(*g*). The mechanism freedom space now resembles that of an articulated wrist mechanism as F_1 and F_2 correspond to pitch and yaw DoFs. The two freedom lines also cannot drift with different displaced orientations. F_3 represents the translation of the End Effector about its central axis as it did when the mechanism was in the nominal configuration. F_4 represents rotation of the End Effector about its central axis, resulting from the small but finite torsional compliance assumption for the compliant strips. Even though this is a DoF as predicted by the constraint analysis, stiffness in this direction is much higher than for the other DoFs. As a result, rotation of the End Effector about its central axis behaves more like a DoC in practice. This example highlights the limitations of a binary treatment of DoF and DoC in constraint analysis.

While intentional compliance provides desired functionality and expands the mechanism design space, it also leads to an inherent set of tradeoffs. Increasing the above torsional compliance of the compliant strips increases the range of articulation but reduces the load-bearing and transmission capabilities of the mechanism. Transmission of an actuation load from the first revolute joints (e.g., $R1_1$) to the End Effector will cause the compliant strip to twist, thereby limiting its torque transmission capability. Also, such twisting means that the DoFs provided by the compliant hinges in $L1_2$ will no longer be parallel and redundant, which impacts the freedom space of the overall mechanism. Similar issues will impact load-bearing capabilities of the mechanism. Loading may also cause the torsional freedom line (e.g., $F1_5$) to drift, which in turn would cause F_1 and F_2 to drift. Furthermore, this mechanism stores energy because of its compliance thereby impacting transmission efficiency. However, with suitable optimization of compliance and geometry, it is possible for this mechanism to achieve close to a full hemispherical range of motion.

The mechanism offers a large open space around the virtual center, making it well-suited for applications that require a human interface [4,5]. In these types of applications, F_3 enables natural adjustability to ensure the user's wrist is centered at the mechanism's center of rotation regardless of hand size.

2.8 BYU Space Pointing Mechanism. The Space Pointing Mechanism is a novel compliant parallel kinematic architecture [12], shown in Fig. 10(*a*) in its nominal configuration. It contains two chains shown in pink and blue that are not identical. A rotary actuator is meant to be connected to each chain via the hexagonal protrusions labeled $M1_1$ and $M2_1$. The first chain, shown in pink, contains four cross-axis flexural pivots, which are meant to approximate revolute joints. $M1_1$ is connected to the first two pivots $H1_1$ and $H1_2$ via rigid link $L1_1$. $H1_1$ and $H1_2$ have collinear axes of rotation. These two flexural pivots are directly connected to the Base,

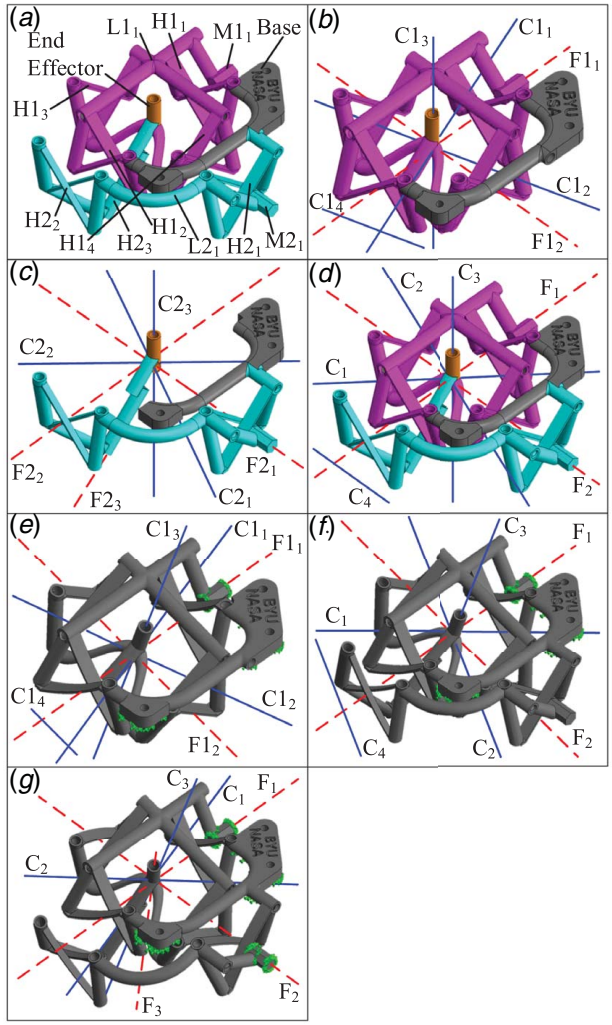

Fig. 10 BYU Space Pointing Mechanism: (*a*) full mechanism nominal configuration, (*b*) first chain nominal configuration, (*c*) second chain nominal configuration, (*d*) full mechanism nominal configuration, (*e*) first chain after rotation about $F1_1$, (*f*) full mechanism after single rotation about F_1, and (*g*) full mechanism after both rotations (Color version online.)

shown in gray. $L1_1$ connects $M1_1$, $H1_1$, and $H1_2$ to the other two flexural pivots $H1_3$ and $H1_4$. $H1_3$ and $H1_4$ also have collinear axes of rotation. These two pivots are directly connected to the End Effector, shown in orange. The second chain, shown in blue, consists of two cross-axis flexural pivots $H2_1$ and $H2_2$ and one split-tube flexure $H2_3$, which also approximates a revolute joint. The chain is arranged B-$H2_1$-$L2_1$-$H2_2$-$H2_3$-EE. M_2 is also connected to $H2_1$ via $L2_1$.

The freedom and constraint spaces of the first chain in the nominal configuration are shown in Fig. 10(*b*). $F1_1$ is provided by both $H1_1$ and $H1_2$, while $F1_2$ is provided by both $H1_3$ and $H1_4$. These two freedom lines are orthogonal and intersect. The corresponding constraint space includes $C1_1$, $C1_2$, and $C1_3$ that are not coplanar and intersect at the intersection of the two freedom lines. $C1_4$ is coplanar to both freedom lines but does not pass through their intersection.

The freedom and constraint spaces of the second chain in the nominal configuration are shown in Fig. 10(*c*). The flexural joints $H2_1$, $H2_2$, and $H2_3$ provide $F2_1$, $F2_2$, and $F2_3$, respectively. It should be noted that while the three freedom lines intersect at a single point, $F2_3$ does not lie in the same plane as the other two freedom lines. This intersection point is shared by the two DoFs from the first chain. $F2_1$ and $F2_2$ are also coplanar to both

freedom lines and collinear to $F1_2$ and $F1_1$, respectively. The corresponding constraint space comprises $C2_1$, $C2_2$, and $C2_3$, which are not all coplanar but share the same intersection point.

The mechanism's constraint and freedom spaces in the nominal configuration are shown in Fig. 10(*d*). The constraint space is identical to the first chain's because the second chain's three DoCs are redundant. Thus, the mechanism's freedom space in its nominal configuration is also identical to the first chain's and the mechanism resembles an articulated wrist mechanism. However, some of the important geometric relationships that make this possible no longer hold in displaced configurations.

The constraint and freedom spaces of the first chain after a single rotation about $F1_1$ are shown in Fig. 10(*e*). $F1_2$ rotates along with the End Effector, and the two freedom lines maintain the same point of intersection and their orthogonal relationship. The plane composed of the two freedom lines also remains orthogonal to the central axis. As expected, the constraint space of the chain also rotates about $F1_1$ but maintains all of the same relationships as in the nominal configuration.

The constraint and freedom spaces for the overall mechanism after a single rotation about F_1 are shown in Fig. 10(*f*). The second chain primarily allows this displacement through deformation of $H2_2$. Thus, the freedom and constraint spaces of the second chain do not change significantly from the nominal configuration. The mechanism's constraint and freedom spaces are therefore dictated again by the corresponding spaces of the first chain and the mechanism appears to remain an articulated wrist mechanism. However, an important result of this rotation is that F_2 (dictated by $F1_2$) is no longer collinear to $F2_1$, which is still the axis of rotation of the actuator connected to the second chain. Given this, for the second actuation about $F2_1$ to happen, $H1_3$ and $H1_4$ would need finite compliance about the two DoCs in each that do not pass through the intersection of $F1_1$ and $F2_1$; this compliance will require twisting along the flexural blades of each pivot. Similarly, $H2_2$ and $H2_3$ would also need to have finite compliance about the two DoCs that do not intersect $F1_1$ for a rotation about $F1_2$ to be possible. A similar issue occurs if the rotations take place in the opposite order.

This analysis shows that if this mechanism were to be composed entirely of joints that are ideal (i.e., completely rigid in their DoCs), it would only be able to rotate along one of the two rotational DoFs at a time. However, this mechanism behaves as an articulated wrist mechanism where both pitch and yaw can be simultaneously actuated if pivots $H1_3$, $H1_4$, $H2_2$, and $H2_3$ have finite compliance along the DoCs specified above. This shows how intentional use of compliance can enable functionality that would otherwise not be possible. With the specified compliance in DoCs, the constraint and freedom spaces of this mechanism after rotations about $F1_1$ and $F2_1$ are shown in Fig. 10(*g*). The introduction of compliance brings an unintended and uncontrolled DoF F_3 but ensures that actuation is possible along $F1_1$ and $F2_1$ (represented by F_1 and F_2). Despite appearing to have the freedom space of a spherical joint, the stiffness about F_3 is significantly higher than about either of the other two DoFs. Consequently, this rotation of the End Effector about the central axis behaves more like a DoC in practice.

While the nature and location of the pitch and yaw freedom lines do not appear to change due to mechanism kinematics, these lines may still drift due to relatively small deformations along DoCs of some of the flexural pivots. This can also lead to these freedom lines not intersecting. The range of motion of this mechanism is tied to the amount of compliance incorporated in the specified DoCs of the flexural pivots. This compliance will also reduce load-bearing and transmission capabilities because loading will cause increasing deformation of the flexural pivots in their DoCs. One instance of this mechanism [12], made monolithically, provided a modest range of motion (~15 deg cone) with moderate to high stiffness expected in its DoCs. While not arranged for an open space around the intersection of its DoFs in the figure, it can be arranged to create this open space. With appropriate tuning of the stiffness of the flexural pivots, this mechanism could be used for applications that require a remote center such as those involving a human interface.

3 Conclusion

The performance attributes of all eight mechanisms are summarized in Table 1. Of these, the nature and location of the two rotational DoFs in the nominal and displaced configurations are two key attributes that allow for a functional categorization of the mechanisms. Mechanisms that provide purely rotational pitch and yaw DoFs that do not translate over their workspace, such as the Dual Arch, Agile Eye, and Tip-Tilt Plate mechanisms, can be used in a wide range of applications that require tracing a constant radius spherical section. However, it is difficult to find or design a parallel kinematic articulated wrist mechanism belonging to this category that is also able to trace an entire hemisphere; mechanisms belonging to this category can typically achieve only a portion of a hemisphere limited by singularities and/or link collisions. This is an important area of future investigation and innovation. Mechanisms in which the nature of the pitch and yaw DoFs change such as the OmniWrist and Three-Spherical Kinematic Chain Parallel Mechanisms are limited to use in applications that either do not require a workspace with constant radius or can compensate for this non-ideal behavior. Mechanisms in which the locations of the pitch and yaw DoFs can drift such as the FlexDex and BYU Space Pointing mechanisms are also similarly limited.

Table 1 Performance attributes of the articulated wrist mechanisms

Mechanism	Total number of DoFs	Location of pitch and yaw DoFs	Nature of pitch and yaw DoFs	Mechanism features that can impact load-bearing and transmission capabilities
Dual Arch	4 (N, D)	On central axis (N, D)	Rotational (N, D)	Link and joint dimensions, range of motion, singular configurations
Tip-Tilt Plate	2 (N, D)	On central axis (N, D)	Rotational (N, D)	Link and joint dimensions, range of motion
Agile Eye	3 (N, D)	On central axis (N, D)	Rotational (N, D)	Link and joint dimensions, range of motion
OmniWrist III	2 (N, D)	On central axis (N, D)	Rotational (N), Screw (D)	Link and joint dimensions, range of motion, number of serial chains
OmniWrist V	2 (N, D)	On central axis (N, D)	Rotational (N), Screw (D)	Link and joint dimensions, number of serial chains
Three-Spherical Kinematic Chain Parallel	3 (N, D)	On central axis (N, D)	Rotational (N), Screw (D)	Link and joint dimensions, number of serial chains
FlexDex	3 (N), 2 (DR), 3 (DF)	On central axis (N), can drift (DF)	Rotational (N, D)	Link and joint dimensions, stiffness of compliant elements
BYU Space Pointing	2 (N), 1 (DR), 2 (DF)	On central axis (N), can drift (DF)	Rotational (N, D)	Link and joint dimensions, stiffness of compliant elements

Note: N, nominal configuration; D, displaced configuration; R, with ideal links and joints; and F, with some flexibility/compliance.

The FlexDex and BYU Space Pointing mechanisms also stand apart for their intentional use of compliance, which enables functionality that may be difficult to achieve using ideal links and joints. However, this approach also leads to tradeoffs, including potential drifting of the location of their rotational DoFs, as noted above. The location of DoFs for such mechanisms can be both orientation-dependent and load-dependent. Compliance also impacts the mechanism's range of motion and load-bearing and transmission capabilities.

Another important design strategy utilized by many of the reported mechanisms is overconstraint, which can be used for several reasons. One reason is to enable ground-mounted actuation, as is the case for the Agile Eye and BYU Space Pointing mechanisms. Another reason is to increase load-bearing capabilities; this can be done for the OmniWrist and Tip-Tilt Plate mechanisms, in which additional serial chains can be added to improve stiffness. Load transmission capability can similarly be improved and also enable the overactuation of DoFs (e.g., providing independent actuators to all four of the OmniWrist III's serial chains). In each of these scenarios, overconstraint is only possible when the additional constraint lines are redundant throughout the mechanism's range of motion. This condition can be met by introducing small clearances into joints or by utilizing compliance. For example, compliance is introduced in the FlexDex mechanism to ensure that constraint lines remain redundant. There are important tradeoffs with either approach, but they can contribute to important performance improvements.

Finally, it is important to note the diversity in mechanisms that can produce similar freedom spaces. For example, both the Dual Arch and FlexDex mechanisms share similar freedom spaces when the FlexDex mechanism's compliant strips are assumed compliant in torsion. Also, the OmniWrist mechanisms, which have distinct architectures, share similar freedom spaces. Despite having similar freedom spaces, each mechanism provides a unique set of performance tradeoffs that makes it better suited for different applications.

Acknowledgment

Revanth Damerla was supported by a National Science Foundation Graduate Research Fellowship during this research.

Conflict of Interest

There are no conflicts of interest.

Data Availability Statement

The datasets generated and supporting the findings of this article are obtainable from the corresponding author upon reasonable request.

References

[1] Salerno, M., Zhang, K., Menciassi, A., and Dai, J. S., 2016, "A Novel 4-DOF Origami Grasper With an SMA-Actuation System for Minimally Invasive Surgery," IEEE Trans. Rob., **32**(3), pp. 484–498.
[2] Navarro, J. S., Garcia, N., Perez, C., Fernandez, E., Saltaren, R., and Almonacid, M., 2010, "Kinematics of a Robotic 3UPS1S Spherical Wrist Designed for Laparoscopic Applications," Int. J. Med. Rob. Comput. Assist. Surg., **6**(3), pp. 291–300.
[3] Schoepp, H., 2013, "Axial Surgical Trajectory Guide," U.S. Patent No. 2013/0066334 A1.
[4] Awtar, S., Trutna, T. T., Nielsen, J. M., Abani, R., and Geiger, J., 2010, "FlexDex™: A Minimally Invasive Surgical Tool With Enhanced Dexterity and Intuitive Control," ASME J. Med. Devices, **4**(3), pp. 1–8.
[5] Awtar, S., and Nielsen, J., 2019, "Parallel Kinematic Mechanisms With Decoupled Rotational Motions," U.S. Patent No. 10,405,936 B2.
[6] Beurrier, H. R., 1968, "Output Control Device With Adjustable Self-Returning Null," U.S. Patent No. 3,394,611.
[7] Shimomura, H., 2000, "Multi-Direction Input Device," U.S. Patent No. 6,078,247.
[8] Rosheim, M. E., 1989, *Robot Wrist Actuators*, Wiley, New York.
[9] Rosheim, M. E., 1994, *Robot Evolution: The Development of Anthrobotics*, Wiley, New York.
[10] Gosselin, C. M., St., Pierre, E., and Gagné, M., 1996, "On the Development of the Agile Eye," IEEE Rob. Autom. Mag., **3**(4), pp. 29–37.
[11] Rosheim, M. E., and Sauter, G. F., 2002, "New High-Angulation Omni-Directional Sensor Mount," Proc. SPIE, **4821**, pp. 163–174, Free-Space Laser Communication Laser Imaging II. 1
[12] Merriam, E. G., Jones, J. E., Magleby, S. P., and Howell, L. L., 2013, "Monolithic 2 DOF Fully Compliant Space Pointing Mechanism," Mech. Sci., **4**(2), pp. 381–390.
[13] Hopkins, J. B., Panas, R. M., Song, Y., and White, C. D., 2017, "A High-Speed Large-Range Tip-Tilt-Piston Micromirror Array," J. Microelectromech. Syst., **26**(1), pp. 196–205.
[14] McNamara, I. E., Toombs, N. J., Kim, J., Mcnamara, D. P., and Rapp, N. L., 2019, "Autonomous Fire Locating and Suppression Apparatus and Method," U.S. Patent No. 2019/0054333 A1.
[15] Hammond, F. L., Howe, R. D., and Wood, R. J., 2013, "Dexterous High-Precision Robotic Wrist for Micromanipulation," 2013 16th International Conference on Advanced Robotics, Montevideo, Uruguay, Nov. 25–29.
[16] Awtar, S., Bernard, C., Boklund, N., Master, A., Ueda, D., and Craig, K., 2002, "Mechatronic Design of a Ball-on-Plate Balancing System," Mechatronics, **12**(2), pp. 217–228.
[17] Liu, G., Gao, J., Yue, H., Zhang, X., and Lu, G., 2006, "Design and Kinematics Simulation of Parallel Robots for Ankle Rehabilitation," 2006 IEEE International Conference on Mechatronics and Automation, Luoyang, Henan, China, June 25–28, pp. 1109–1113.
[18] Dai, J. S., Zhao, T., and Nester, C., 2004, "Sprained Ankle Physiotherapy Based Mechanism Synthesis and Stiffness Analysis of a Robotic Rehabilitation Device," Auton. Rob., **16**(2), pp. 207–218.
[19] Saglia, J. A., Dai, J. S., and Caldwell, D. G., 2008, "Geometry and Kinematic Analysis of a Redundantly Actuated Parallel Mechanism That Eliminates Singularities and Improves Dexterity," ASME J. Mech. Des., **130**(12), p. 124501.
[20] Blanding, D. L., 1999, *Exact Constraint: Machine Design Using Kinematic Principles*, ASME Press, New York.
[21] Hunt, K. H., 1979, *Kinematic Geometry of Mechanisms*, Oxford University Press, New York.
[22] McCarthy, J. M., and Soh, G. S., 2011, *Geometric Design of Linkages*, Springer, New York.
[23] Huang, Z., and Li, Q. C., 2002, "General Methodology for Type Synthesis of Symmetrical Lower-Mobility Parallel Manipulators and Several Novel Manipulators," Int. J. Rob. Res., **21**(2), pp. 131–145.
[24] Zhao, J. S., Zhou, K., and Feng, Z. J., 2004, "A Theory of Degrees of Freedom for Mechanisms," Mech. Mach. Theory, **39**(6), pp. 621–643.
[25] Dai, J. S., Huang, Z., and Lipkin, H., 2006, "Mobility of Overconstrained Parallel Mechanisms," ASME J. Mech. Des., **128**(1), pp. 220–229.
[26] Hopkins, J. B., 2010, *Design of Flexure-Based Motion Stages for Mechatronic Systems via Freedom, Actuation and Constraint Topologies (FACT)*, Massachusetts Institute of Technology, Cambridge, MA.
[27] Kong, X., and Gosselin, C. M., 2004, "Type Synthesis of 3-DOF Spherical Parallel Manipulators Based on Screw Theory," ASME J. Mech. Des., **126**(1), pp. 101–108.
[28] Zhang, K., Fang, Y., Fang, H., and Dai, J. S., 2010, "Geometry and Constraint Analysis of the Three-Spherical Kinematic Chain Based Parallel Mechanism," ASME J. Mech. Rob., **2**(3), p. 031014.
[29] Rosheim, M. E., 2003, "Robotic Manipulator," U.S. Patent No. 6,658,962 B1.
[30] Rosheim, M. E., 2017, "Robot Manipulator With Spherical Joints," U.S. Patent No. 9,630,326 B2.
[31] Damerla, R., and Awtar, S., 2020, "Constraint-Based Analysis of Parallel Kinematic Articulated Wrist Mechanism," *ASME IDETC/CIE* 2020.
[32] Damerla, R., 2020, *Constraint-Based Analysis of Parallel Kinematic Articulated Wrist Mechanism*, University of Michigan, Ann Arbor, MI.
[33] Shi, Z. Y., Liu, D., and Wang, T. M., 2014, "A Shape Memory Alloy-Actuated Surgical Instrument With Compact Volume," Int. J. Med. Robot. Comput. Assist. Surg., **10**(4), pp. 474–481.
[34] Bonev, I. A., Chablat, D., and Wenger, P., 2006, "Working and Assembly Modes of the Agile Eye," Proceedings—IEEE International Conference on Robotics and Automation, Orlando, FL, May 15–19, pp. 2317–2322.